Cryobiology 114 (2024) 104839

Contents lists available at ScienceDirect

Cryobiology

journal homepage: www.elsevier.com/locate/cryo

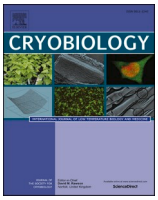

Direct comparison of isobaric and isochoric vitrification of two aqueous solutions with photon counting X-ray computed tomography

Jason T. Parker [1,**], Anthony N. Consiglio [1,*], Boris Rubinsky, Simo A. Mäkiharju

Department of Mechanical Engineering, University of California, Berkeley, Berkeley, CA, 94720, USA

A B S T R A C T

Vitrification is a promising approach for ice-free cryopreservation of biological material, but progress is hindered by the limited set of experimental tools for studying processes in the interior of the vitrified matter. Isochoric cryopreservation chambers are often metallic, and their opacity prevents direct visual observation. In this study, we introduce photon counting X-ray computed tomography (CT) to compare the effects of rigid isochoric and unconfined isobaric conditions on vitrification and ice formation during cooling of two aqueous solutions: 50 wt% DMSO and a coral vitrification solution, CVS1. Previous studies have only compared vitrification in isochoric systems with isobaric systems that have an exposed air-liquid interface. We use a movable piston to replicate the surface and thermal boundary conditions of the isochoric system yet maintain isobaric conditions. When controlling for the boundary conditions we find that similar ice and vapor volume fractions form during cooling in isochoric and isobaric conditions. Interestingly, we observe distinct ice and vapor cavity morphology in the isochoric systems, possibly due to vapor outgassing or cavitation as rapid cooling causes the pressure to drop in the confined systems. These observations highlight the array of thermal-fluid processes that occur during vitrification in confined aqueous systems and motivate the further application of imaging techniques such as photon counting X-ray CT in fundamental studies of vitrification.

1. Introduction

The ability to preserve biological systems such as cells, plants, organs, and even entire organisms for indefinite periods of time has remained an elusive goal of the biomedical and conservation communities as traditional clinical methods only enable the storage of organs for a few hours [1] and cryo-banking of full organisms is generally not possible. The significant challenge of preserving biological systems outside of their normal environment stems from the requirement of either 1) maintaining normal physiological processes that support metabolic activity [2,3] or 2) suppressing metabolic processes to prevent deterioration. Metabolism, which represents the sum of enzymatic reactions that sustain life, is largely an Arrhenius process, and as such, is a strong function of temperature. At cryogenic temperatures, molecular processes are arrested to such an extent as to bring about a state of suspended animation.

The greatest challenge facing successful cryopreservation is avoiding the formation of ice, which is nearly universally lethal to biological systems through various mechanical, chemical, and osmotic mechanisms [4]. Vitrification involves the solidification of a liquid not by crystallization but rather through formation of a glass whereby an increase in viscosity results in arrested molecular motion and suppressed ice nucleation. Vitrification therefore represents a compelling method for ice-free cryopreservation. However, the nucleation rate of ice in aqueous solutions is a steep function of supercooling, and cooling rates exceeding 10^6 °C/s are required to vitrify water [5,6]. The addition of solutes, termed cryoprotective agents (CPAs), and the application of pressure affect both equilibrium and non-equilibrium freezing processes and lower the cooling rate needed to achieve glass formation [7]. At the concentrations needed to effectively suppress ice nucleation, many CPAs are toxic, further complicating the application of vitrification and motivating the search for new methods to achieve stable ice-free cryopreservation.

Recently, rigid isochoric confinement has been found to reduce the likelihood of ice nucleation in supercooled water by providing isolation from external perturbations, removing exposed liquid-air interfaces, and potentially imparting an energetic toll upon incipient ice embryos as they expand relative to the liquid phase [8–11]. Confinement may also alter ice growth dynamics since the formation of ice in a confined volume acts to self-pressurize the system, which shifts the phase equilibrium and can result in arrested crystallization dynamics and two-phase solid-liquid equilibrium [12].

* Corresponding author.
** Corresponding author.
E-mail addresses: jtparker@berkeley.edu (J.T. Parker), aconsiglio4@berkeley.edu (A.N. Consiglio).
[1] These authors contributed equally.

https://doi.org/10.1016/j.cryobiol.2023.104839
Received 2 October 2023; Received in revised form 29 November 2023; Accepted 8 December 2023
Available online 12 December 2023
0011-2240/© 2023 The Authors. Published by Elsevier Inc. This is an open access article under the CC BY-NC-ND license (http://creativecommons.org/licenses/by-nc-nd/4.0/).

Isochoric systems have also received attention for their potential to improve cryopreservation outcomes by promoting vitrification. In an exploratory study, Zhang et al. [13] monitored pressure during cooling as an indicator for ice formation and found that concentrations lower than the critical values reported in the literature vitrified in isochoric systems without an increase in pressure. Solanki and Rabin subsequently proposed in a computational study that contraction of an aqueous solution during cooling would generate vapor cavities within the isochoric container, enabling the absence of a pressure rise in the presence of certain ice fractions and potentially explaining the previous observations [14]. More recently, Powell-Palm et al. [15] employed an isochoric system in order to successfully vitrify and revive centimeter-scale coral specimens, representing an important cryo-conservation milestone. To the best knowledge of the authors, Powell-Palm et al. [15] are the only group to experimentally compare rigidly confined isochoric and unconfined isobaric vitrification of aqueous systems. That study compares an enclosed isochoric chamber to an open chamber with an exposed air-liquid interface. As a result, the heat transfer and surface conditions are not matched between the isochoric and isobaric configuration. Comparing vitrification in confined and unconfined systems with matched heat transfer and surface conditions has remained unexplored.

Motivated by the promising vitrification result of Powell-Palm et al. [15] and the still poorly understood process of vitrification in confined systems, we adapted our custom-built photon counting CT system [20, 21] to conduct photon counting X-ray computed tomography (CT) measurements of two aqueous solutions cooled at rates of roughly 100 °C/min in liquid nitrogen (50 wt% dimethyl sulfoxide (DMSO) and the coral vitrification solution (CVS1) [15]), each under isochoric (rigidly confined) and isobaric (unconfined) conditions. This technique uses a laboratory-scale X-ray system to resolve phase segregation inside rigid metallic chambers at $O(100\ \mu m)$ reconstructed resolution and captures the full aqueous volume in a single scan.

We find that vitrification of 50 wt% DMSO leads to an inward tapered interface in both isochoric and isobaric configurations, which is a result of thermal contraction of the fluid. In the isochoric system the chamber pressure drops as the fluid contracts and a vapor cavity (or cavities) forms through either outgassing or cavitation. The CVS1 solution is found to partially crystallize in nearly equal amounts when cooled at 100–120 °C/min in both isochoric and isobaric conditions. Distinct ice morphologies are observed in CVS1 between the isochoric and isobaric-piston configurations, potentially resulting from similar cavity formation processes as in the 50 wt% DMSO solution – namely, outgassing or cavitation. These observations highlight the role of thermal-fluid processes in the vitrification of confined aqueous systems and pave the way for future investigations of ice nucleation, growth, and vitrification processes using imaging techniques such as photon counting X-ray CT.

2. Materials and methods

2.1. Discussion of isochoric and isobaric processes and terminology

The diverse applications of isochoric systems in cryopreservation has the potential to lead to inconsistent interpretations of isochoric processes. One challenge stems from the use of isochoric systems in multiple cryopreservation modalities, namely freezing, supercooling, and vitrification. The first mode, isochoric freezing, is exemplified by a self-pressurization that occurs when ice grows and expands within a rigid container, which depresses the equilibrium water-ice phase transition temperature and results in a stable two-phase equilibrium. Conversely, the second and third mode of isochoric systems, supercooling and vitrification, aim to stabilize the liquid or glassy state, respectively, solely through the effect of rigid confinement. Both modalities act in the absence of the equilibrium-shifting self-pressurization imparted by confined ice growth. Additional hybrid scenarios are also possible, including vitrification with partial ice growth, one variation of which has been termed “self-pressurized rapid freezing” [16].

A second challenge pertains to the strictness of the terms isochoric and isobaric, which mean constant volume and constant pressure, respectively. These terms are often used in reference to statistical mechanical ensembles that provide a theoretical framework for describing the thermodynamic properties of a system in terms of thermodynamic variables such as energy, entropy, temperature, pressure, volume, etc., or to describe thermodynamic equilibrium states, which can be analyzed using isochoric or isobaric phase diagrams. Additionally, all materials possess finite compressibility and, generally, finite thermal expansivity and thus cannot truly be of constant volume. Similarly, all finite systems experience pressure fluctuations and cannot be considered strictly isobaric. In brief, systems exist on a spectrum between the two extremes and may be more conveniently analyzed in one framework depending on the conditions of an experiment.

With these two points in mind, we may consider how different vitrification scenarios can be described as either isochoric or isobaric. As a starting interpretation, we might label any vitrification process occurring inside a rigid container as isochoric vitrification. This interpretation perhaps describes the device employed and thermodynamic state of the system but fails to distinguish whether additional processes, such as pressurization, ice growth, or vapor formation, are simultaneously occurring and does not quantify the qualifier for rigidity.

An alternate interpretation may draw an analogy to the underlying motivation for conducting supercooling in an isochoric system: initial ice formation and subsequent growth of ice from the liquid state is accompanied by a pressure increase that shifts the phase equilibrium and thus imparts an energetic toll on ice inception and growth, and that rigid confinement also isolates the system from external perturbations. In order for this confinement effect to be present, two conditions must be maintained during the vitrification process. The first condition,

$$V_{aq}(T,P) = V_{c,in}(T,P), \tag{1}$$

requires that the aqueous material fills the entire free container volume. Here, $V_{aq}(T,P)$ is the volume of the aqueous phase, $V_{c,in}(T,P)$ is the container inner volume, T is temperature, and P is pressure. If part of the container volume is occupied by a vapor phase or another compressible element, then the aqueous phase will be able to freely expand or contract. Thus, a second condition must be that:

$$\beta_{c,eff} \ll \beta_{aq}. \tag{2}$$

This condition requires that the confinement be much more rigid than the aqueous phase. Here, β_{aq} is the compressibility of the aqueous phase, and $\beta_{c,eff}$ is the *effective* compressibility of the confinement, where $\beta \equiv \frac{1}{V}\left(\frac{\partial V}{\partial P}\right)$. This effective compressibility depends on the geometry of container and is thus not solely dependent on its material properties.

These two conditions ensure that the aqueous phase is in mechanical communication with container and that the container is sufficiently rigid. It is not possible at this time to provide a quantitative limit for the confinement rigidity, and so the second condition is qualitatively formulated to stress relevant system properties. A good rule of thumb, however, may be an order of magnitude difference or more.

If these two conditions are violated, then the aqueous phase will not experience rigid confinement. This may occur, for example, if a vapor phase is present within the container. In this case, the non-crystalline aqueous phase would not have the same volume as its container and would not experience the rigid confinement effect until the vapor phase is compressed significantly. Similarly, if the aqueous phase fills the entire container volume but the container is flexible, then the container will expand in response to ice growth and not impart a significant restoring force.

As will become important in the remainder of this study, in order to prevent the formation of a vapor phase, the pressure in the aqueous solution must not drop below a certain critical pressure, P_{cr}, at which vapor forms through outgassing or cavitation. This critical pressure will

differ depending on the vapor formation mechanism and is likely a function of the rate of pressure change and dissolved gas content. By considering the thermal contraction and fluid compressibility, we can derive a first order estimate of the pressure inside an isochoric system as a function of temperature:

$$P(T) = P_0 + \frac{1}{\beta_{aq}(T)}\left[1 - \exp\left(\int_{T_0}^{T}\left(\alpha_c(\tau) - \alpha_{aq}(\tau)\right)d\tau\right)\right], \quad (3)$$

where $\alpha_c(T)$ and $\alpha_{aq}(T)$ are the temperature dependent thermal expansion coefficients of the container and aqueous phase, respectively, and P_0 is the initial system pressure. As detailed in the Supplemental Information, this model follows from several assumptions such as the thermal expansion coefficient and compressibility being only a function of temperature and not pressure, the absence of temperature or pressure gradients, and no phase change. According to this model, the pressure decreases upon cooling (i.e., $\frac{dP}{dT} < 0$) when the aqueous phase contracts more than the container. The pressure must remain above the critical pressure in order to avoid vapor cavity formation and thus the loss of isochoric confinement during vitrification. As the solution viscosity increases in the vicinity of the glass transition temperature, the solution is considered viscoelastic and its stress state cannot be fully described by Equation (3). A detailed numerical model of this scenario in system 7.05 M DMSO was developed by Solanki and Rabin [14].

This discussion has sought to highlight the variety of isochoric processes as well as identify potential conditions necessary for vitrification to be carried out under the effects of confinement. These systems exist on a spectrum and cannot easily be defined with hard limits. They may also not fit strictly into one definition. Self-pressurized freezing that is accompanied by vitrification is a example of such a system [16]. Such hybrid processes present additional complexities that likely will require development of a new vernacular within the cryopreservation community. The authors hope that the proposed definitions will spur further discussion in the literature.

For the purpose of this study, the use of the terms “isochoric” and “isobaric” when describing system configurations aligns most closely with the thermodynamic equilibrium state of the system. This point will become clearer in the following sections in which initially rigidly confined systems are labeled as isochoric and non-rigidly confined and open systems in which the aqueous phase is ultimately able to expand are labeled as isobaric.

2.2. Vitrification solutions

We selected two aqueous solutions as the focus of these exploratory experiments. The first solution is a common binary glass-forming aqueous solution consisting of 50 wt% DMSO in deionized water. This solution has a well-characterized and easily achievable critical cooling rate of $\leq$5 °C/min [17], which enables us to isolate the effects of isochoric confinement on solution contraction in the absence of ice formation as well as evaluate previous computational models of thermo-mechanical processes during vitrification [14,18,19]. The second solution, known as CVS1, was used in isochoric systems by Powell-Palm et al. [15] to cryopreserve whole coral specimens and is selected in order to provide insights into this promising cryopreservation result. The CVS1 solution consists of 1.05 M DMSO, 1.05 M propanediol, 1.05 M glycerol, and 0.85 M trehalose in physiological buffered saline (PBS) (see Supplemental information for the ingredient weight fractions). Since CVS1 is comprised of multiple traditional CPAs as well as a disaccharide, the critical cooling rate is difficult to estimate *a priori*. Previous studies have not rigorously characterized the critical cooling rate of CVS1, but cooling at roughly 100 °C/min was found to yield positive outcomes during the coral cryopreservation [15]. The experiments presented herein aim to investigate vitrification processes in this newly employed solution.

2.3. Vitrification chambers

Fig. 1 depicts the three systems employed in this study. The main chamber body, constructed of aluminum-7075, has an inner diameter of 12.7 mm (0.5″), an outer diameter of 34.9 mm (1–3/8”), and a nominal internal volume of 5.3 ml. Detailed dimensions of the vitrification chamber are provided in Fig. S7 of the Supplemental Information. Multiple chambers are used throughout the experiments, and all have either anodized or naturally oxidized surfaces. An aluminum threaded plug with a metal-on-metal tapered sealing surface provides rigid confinement for the isochoric trials, as shown on the left in Fig. 1. Due to the thermal contraction of aluminum, the internal chamber volume contracts by approximately 1.5 % during cooling in liquid nitrogen. We measure the volume of the chamber after contraction using photon counting X-ray CT. In order to study the solutions under unconfined isobaric conditions, we introduce two additional configurations. In the first configuration (Fig. 1 right), the liquid interface is open to air and the chamber is covered with Kapton tape to prevent the intrusion of liquid nitrogen during cooling. This configuration allows the liquid interface to freely deform and is similar to systems modeled in previous simulations of thermo-mechanical processes during vitrification [18, 19]. In trials with CVS1 in this configuration, we observed that slower cooling rates near the top surface of the fluid, which is not directly in contact with the metallic chamber, resulted in significant ice formation (see Fig. 6), growing vertically out of the field of view of the X-ray detector. This observation and our desire to examine effect of matching thermal and surface boundary conditions of the isochoric plug motivated the introduction of the second isobaric configuration (Fig. 1 center), which employs a vertically unconstrained aluminum piston. To ensure that no air is trapped underneath the piston, the face of the piston (or plug in the isochoric configuration) is wetted with the solution prior to insertion into the chamber. Solution is drawn out from the TC hole (used as weep hole) with a syringe after the plug is inserted. A preliminary X-ray image is captured prior to cooling to confirm that no bubbles are present.

The three configurations in this study each correspond to the different manifestations of the isochoric and isobaric vitrification scenarios discussed in section 2.1. The isochoric chamber provides initial isochoric confinement by using a sealed aluminum chamber filled entirely with the aqueous solution. The isobaric-piston configuration maintains volume equivalence, but effectively removes the rigid confinement ($\beta_{c,eff} \rightarrow \infty$). Lastly, in the isobaric-Kapton configuration, the aqueous phase is not fully encapsulated by its container and is free to expand or contract without rigid confinement. As discussed in detail in section 2.1, these identifiers conform most closely with the thermodynamic equilibrium descriptions. Whether dynamic vitrification or ice growth processes are affected by confined geometries of otherwise open systems is an open question that future studies should investigate.

2.4. Vitrification procedure

In order to facilitate rapid cooling, we lower a chamber in a vertical orientation O(10 cm/s) to the bottom of a 20–30 cm deep liquid nitrogen bath. The temperature is monitored during this process with a type-T thermocouple inserted into the wall of the chamber, as indicated in Fig. 1, and recorded with an Omega TC-08 thermocouple data logger (with a manufacturer specified uncertainty of ±1 °C). Due to the size and thermal mass of the systems, thermal gradients are present during the plunge cooling, and we utilize this temperature measurement as a rough indicator of a chamber’s thermal history. The average cooling rate for each trial (computed from the recorded temperature measurement between 0 °C and −150 °C) is reported in Table 1. We conduct three repetitions for each condition to account for potential variability in assembly condition and cooling profile. After thermal equilibration in the liquid nitrogen, the chamber is quickly transferred to the X-ray CT station. Here, the chamber is placed into a beaker that sits atop a stack of

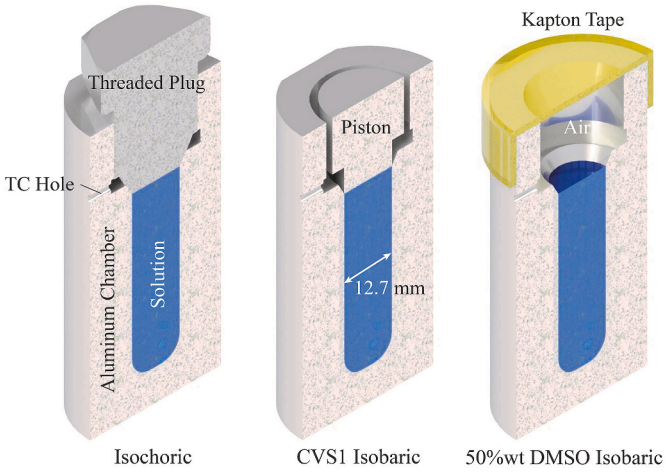

Fig. 1. Vitrification chambers. A two-piece assembly with metal-on-metal sealing surfaces generates rigid initial isochoric confinement (left). Replacing the rigid plug with a movable aluminum piston (center) produces isobaric conditions while resulting in nominally equivalent thermal and surface conditions as the isochoric system. This configuration is employed in the trials with CVS1. Critical cooling rates of ≤5 °C/min are easily achievable with 50 wt% DMSO, and the solution is left uncovered in order to allow the free interface to deform. In this configuration (right), the chamber is capped with Kapton tape to prevent intrusion of liquid nitrogen during cooling. Temperature is monitored using a type-T thermocouple inserted partially into the side of the chamber (TC hole).

three linear stages and one rotation stage. The beaker is partially filled with liquid nitrogen below the chamber to ensure the chamber does not warm over the duration of the CT scan but without obstructing the main field of view. A styrofoam cover is also placed on top of the beaker to prevent convective exchange. In preliminary experiments the temperature of the chamber was measured after completion of the CT scan and was found to never exceed −140 °C.

Table 1
Average cooling rates (°C/min) during plunge cooling in liquid nitrogen of CVS1 and 50 wt% DMSO under isochoric and isobaric conditions. Chamber configurations are depicted in Fig. 1.

	CVS1			50 wt% DMSO	
	Isochoric	Isobaric (piston)	Isobaric (Kapton)	Isochoric	Isobaric (Kapton)
Trial 1	120	108	119	112	109
Trial 2	106	117	134	116	120
Trial 3	100	104	114	110	127
Average	110	109	122	113	119

2.5. Photon counting X-ray computed tomography

Fig. 2 depicts the X-ray CT setup, which consists of a YXLON FXE225.48 X-ray source used in concert with a Dectris Pilatus3 100K-M photon counting detector. Photon counting detectors (PCDs) achieve a higher signal-to-noise ratio than conventional X-ray detectors [20], making them advantageous for collecting CT scans of systems with low X-ray contrast such as multiphase vitrified systems. Lower energy photons, which are more likely the result of scatter and thus introduce noise, can also be rejected with PCDs. That PCDs are photon energy-resolving detectors instead of the traditional photon energy-integrating detectors is the primary advantage and the root of their benefits. The energy threshold for these experiments is set at a nominal 20 keV with a 10 keV threshold roll-off setting on the Pilatus3 detector. We collect 114 projections per CT scan, each with a 9999.05 ms integration time and a 0.95 ms dead time for a total imaging period of 10 s per projection. The rotation rate is constant at 0.316 degrees per second.

The X-ray source emits a polychromatic cone beam, which produces geometric magnification based on the positions of the object and the detector relative to the source. The magnification factor, M, is the ratio

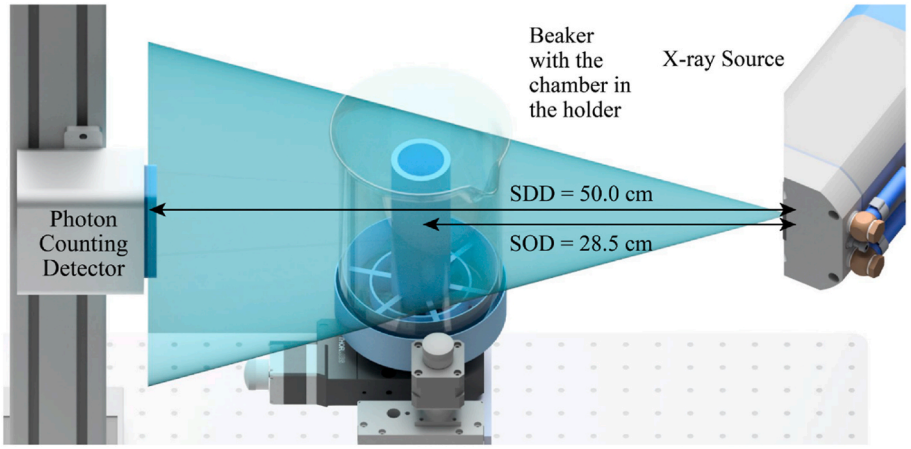

Fig. 2. Experiment setup consisting of a cone beam X-ray source and a photon counting detector. After cooling in a separate dewar of liquid nitrogen, the chamber is placed into a beaker that sits atop a stack of three linear stages and one rotation stage. The beaker is partially filled with liquid nitrogen below the chamber and covered with styrofoam at the top (not pictured) to ensure the chamber does not warm over the duration of the CT scan but without obstructing the main field of view.

between the source-to-detector distance (SDD) and the source-to-object distance (SOD). Based on a magnification factor of M = 1.75 and a pixel size of 172 μm square, we achieve a spatial resolution of 98 μm square for a single projection. Gaining higher spatial resolution sacrifices the field of view, however, reducing the nominal detector area of 8.38 cm high by 3.35 cm long to an effective field of view measuring 4.79 cm high by 1.91 cm long. Although a 98 μm square projection spatial resolution is achieved, the true reconstructed spatial resolution is likely lower due to the relatively few projections captured. The reconstructed resolution is $O(100\ \mu m)$.

We operate the X-ray source at an acceleration voltage of 80 kVp and a target current of 0.8 mA. Based on the manufacturer's specifications, the focal spot for the source at these settings is approximately 87.5 μm full-width half-max. With geometric magnification, we expect the focal blurring to be approximately 153 μm. This is less than the size of a single pixel, so we do not expect notable focal blurring artifacts. Further details on the X-ray imaging setup we use can be found in Refs. [21,22].

2.6. Phase identification

We use the filtered back projection algorithm in the ASTRA Toolbox [23,24] to reconstruct the CT scans onto a 195 x 195 x 487 grid with (98 μm)^3 voxels. A normalization ring artifact correction is applied with a standard deviation of 10 pixels. We then segment the phases in ORS Dragonfly [25] based on their voxel intensity in order to calculate their respective volumes and assess morphology. A 3D median filter with a span of 5 voxels is used to enhance the contrast between ice and the vitrified solution. We do not median filter the vapor cavity scans because there is already sufficient contrast.

Fig. 3 depicts the normalized voxel intensity histograms for the entire reconstructed volume of CVS1 and 50 wt% DMSO under isochoric and isobaric conditions, respectively. Many readers may be more familiar with an inverted intensity scale compared to the scale we present in Fig. 3. We retain the original projection intensity scale, though, in order to demonstrate that the ice and vapor phases attenuate fewer X-rays than the liquid phase (by virtue of being less dense) and thus appear brighter in the captured images. These images demonstrate the contrast between ice, vapor, and vitrified solution with multiple peaks visible. Starting from the left: the first is the aluminum chamber walls; the second is the vitrified solution and, in the CVS1 solution, ice; the third is a vapor cavity, which is only present in the 50 wt% DMSO solution. The difference in the 50 wt% DMSO and CVS1 vitrified solution peaks is due to the higher X-ray attenuation of the 50 wt% DMSO solution compared to CVS1 across the range of photon energies (see Supplemental Information Fig. S1). In this depiction, the ice voxels in the CVS1 solution are hidden within the vitrified solution peak. Fig. 4 depicts the histogram of a single unfiltered slice that contains ice in a CVS1 isochoric scan, revealing the distinction between ice and the surrounding vitrified solution. Each phase is segmented from the others by establishing thresholds at the local minimum between peaks.

3. Results and discussion

3.1. Vitrification of 50 wt% DMSO

The 50 wt% DMSO solution vitrifies completely with cooling rates exceeding 5 °C/min and is selected for investigating thermal contraction behavior. Trials with this solution in the isobaric-piston configuration were not conducted because the slow critical cooling rate obviates the need for heat transfer optimization. Fig. 5 depicts representative 3D reconstructions of the vitrified 50 wt% DMSO solution in isochoric and isobaric-Kapton configurations. All reconstructions are available in the Supplemental Information Figs. S2 and S3. A contracting taper morphology is observed in both conditions and is very similar to deformations observed in previous computational studies of vitrifying systems with free surfaces [18,19]. Average vapor volume fractions of

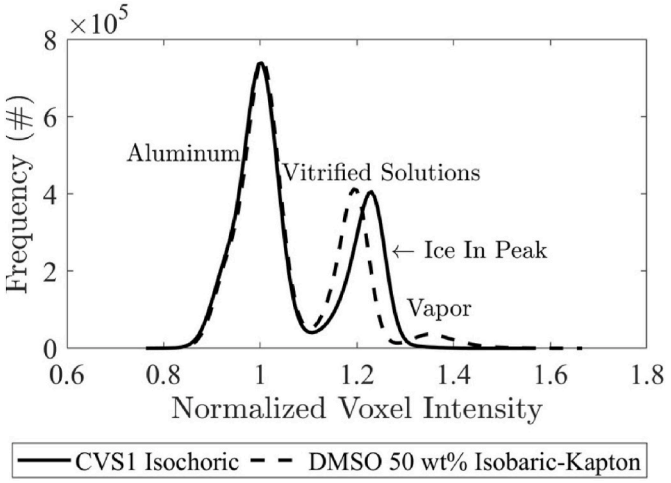

Fig. 3. Normalized voxel intensity histograms of the CT scan reconstruction for the entire volume of CVS1 and 50 wt% DMSO rapidly cooled in liquid nitrogen in isochoric and isobaric-Kapton configurations, respectively. These histograms illustrate the contrast between the aluminum chamber, the vitrified solution, and the vapor phases. The histograms are aligned based on the aluminum peaks.

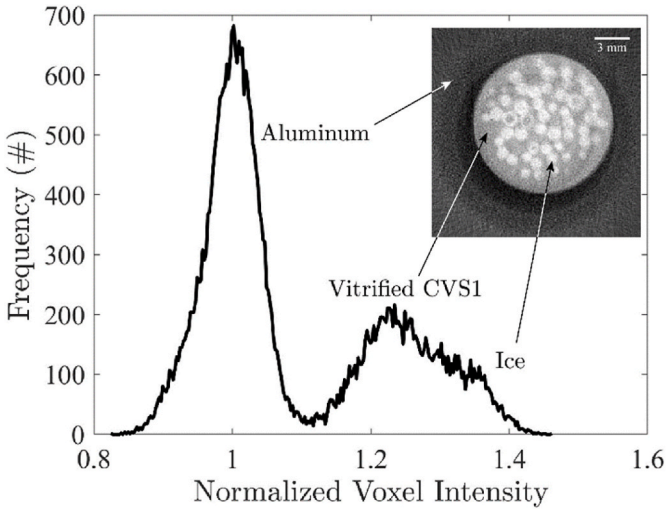

Fig. 4. Voxel intensity histogram of a CT scan reconstruction for a single unfiltered slice of CVS1 rapidly cooled under isochoric conditions. Peaks are visible for the three present phases: aluminum, vitrified CVS1, and ice. Inset depicts the unfiltered reconstructed slice with globular ice morphology.

5.7 % and 6.7 % are computed for the isochoric and isobaric conditions, respectively. Table 2 reports the volume fractions of vapor from each trial. As predicted by the recent computational study by Solanki and Rabin [14], vapor cavities are observed to form during cooling of DMSO solutions in the isochoric chamber. The solution contracts more than the chamber, causing the pressure to drop below the saturation pressure and results in the rejection of dissolved gasses or, if the pressure drops quickly enough, vapor cavitation. The formation of a vapor cavity nullifies the original isochoric confinement.

Interestingly, while the vitrified solution is pinned at the brim of the chamber in the isobaric system, a thin film of vitrified solution is found to remain over the entire inner surface of the isochoric system. This potentially results from surface tension affects between aqueous solution and hydrophilic chamber surface. The sharp interface in the isobaric system may serve as a local stress concentration and could be susceptible to fracturing upon rapid rewarming [18]. Such stresses may be

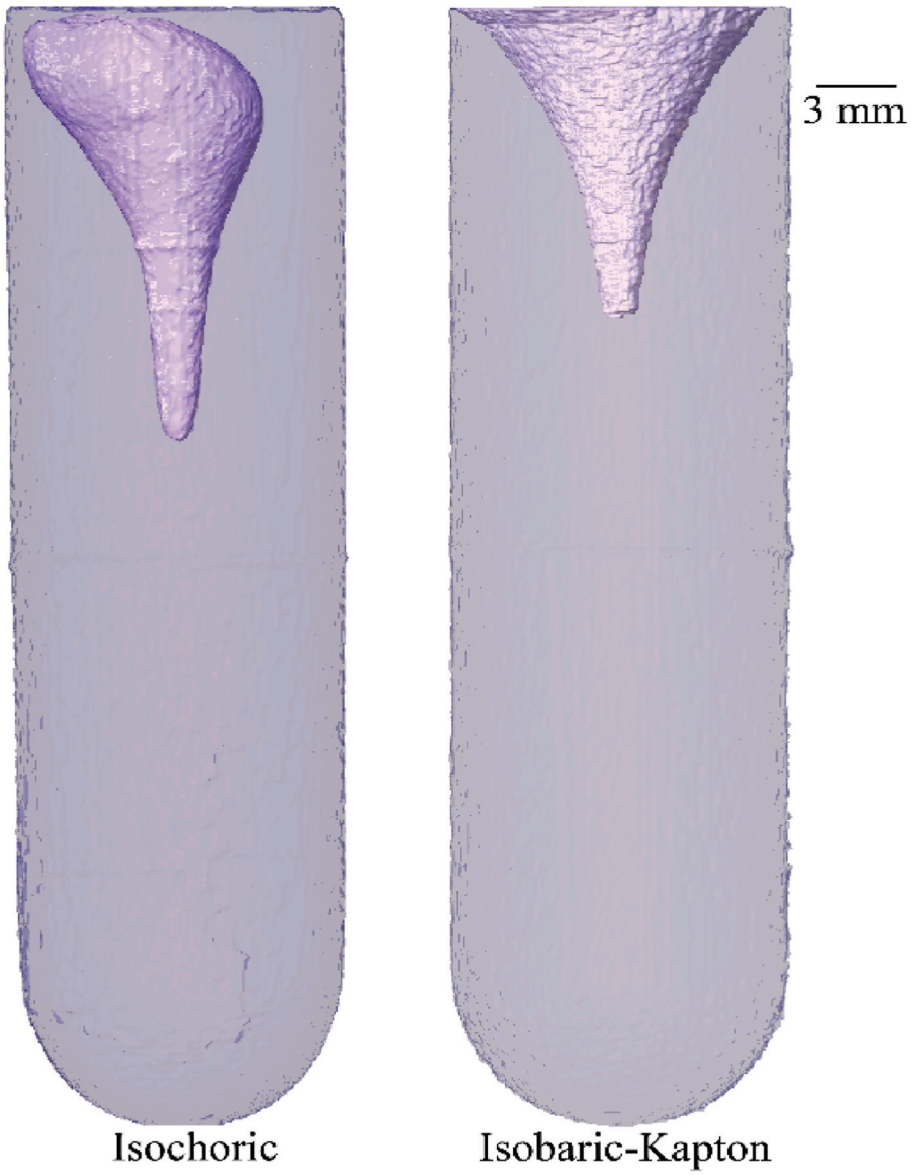

Fig. 5. Reconstructed CT scans of 50 wt% DMSO vitrified under isochoric (left) and isobaric-Kapton (right) conditions. Solution contraction leads to surface deformation and, in the isochoric system, vapor cavity formation. Vitrified solution and vapor phases are segmented and shown in purple and white, respectively. While the vitrified solution is pinned around the brim of the chamber in the isobaric system, a film of vitrified solution covers the entire interior surface of the isochoric system. Vapor volume fractions are reported in Table 2. (For interpretation of the references to colour in this figure legend, the reader is referred to the Web version of this article.)

ameliorated by the smooth interfaces in the isochoric system. The current study only considers static equilibrium systems at cryogenic temperatures; future studies may expand on this and look into how these differences in vitreous interface formation affect glass stability upon rewarming in isobaric and isochoric systems.

Table 2
Volume fractions (%) of ice for the CVS1 trials and of vapor for the 50 wt% DMSO trials. Chamber configurations are depicted in Fig. 1. Representative CT reconstructions are shown in Figs. 5 and 6.

	Ice fraction - CVS1		Vapor fraction - 50 wt% DMSO	
	Isochoric	Isobaric (piston)	Isochoric	Isobaric (Kapton)
Trial 1	0.33	0.53	5.8	5.2
Trial 2	0.44	0.75	5.5	8.9
Trial 3	0.90	1.07	5.9	6.1
Average	0.56	0.78	5.7	6.7

3.2. Ice formation during vitrification of CVS1

Due to its lower molarity, CVS1 has a higher critical cooling rate and a lower coefficient of thermal expansion than the 50 wt% DMSO solution. It is therefore well suited for investigating the potential for isochoric confinement to promote vitrification. The CVS1 solution is cooled following the protocol employed in Powell-Palm et al. [15] resulting in average cooling rates of about 110 °C/min (see Table 1). Despite this protocol enabling cryopreservation and revival of coral specimens (in the isochoric configuration), we find that a small amount of ice crystallizes during cooling.

Fig. 6 shows representative 3D reconstructions of the ice formed in CVS1 in the isobaric-piston, isochoric, and isobaric-Kapton systems. All reconstructions are available in the Supplemental Information Figs. S4–S6. As discussed previously, a significant amount of ice forms in the isobaric-Kapton configuration because the exposed liquid interface does not receive the same direct cooling from the highly conductive

aluminum chamber. This observation motivated the introduction of a movable piston to replicate the thermal boundary condition from the isochoric system while maintaining isobaric conditions. When controlling for the cooling profile in this way, we find that isochoric and isobaric-piston conditions yield similar amounts of ice (on average 0.56 % and 0.78 %, respectively). The volume fractions of resolvable ice formed in each trial are reported in Table 2. It is worth noting that the volume fractions are computed based on resolvable phase segregation at a reconstructed resolution $O(100\ \mu m)$. The nucleation rate of ice is known to reach a maximum at temperatures close to the glass transition temperature while the rate of ice crystal growth rapidly slows at much higher temperatures. During vitrification, this results in the potential for sub-micron crystals that nucleate at very low temperatures but cannot grow to an appreciable size due to the slowed growth kinetics [26]. Future efforts should seek to increase the spatial resolution in order to resolve smaller ice crystals.

Despite finding similar ice volume fractions in CVS1 between the isochoric and isobaric-piston configurations, we do observe morphological differences in the ice that forms. Fig. 7 depicts close-up reconstructions of the segmented ice phases in CVS1 for both conditions. The ice forms near the surface at the gravitational top of the chamber in both conditions. We conducted one experiment with an inverted isochoric system and found that the ice still formed at the gravitational top, suggesting that the observed ice is not a result of geometrical differences between the round bottom and flat lid. Whereas the ice in the isobaric system formed one continuous mass, the ice in the isochoric system formed many millimeter-scale globular crystals. This difference could be the result of outgassing or cavitation [27,28]. Under isochoric confinement the pressure in the chamber drops as the solution contracts during cooling. As the pressure drops below the equilibrium vapor pressure dissolved gasses may be forced out of solution. If the pressure drops rapidly enough, the solution may cavitate. Both possibilities are noted by Solanki and Rabin [14]. Vapor bubbles may then serve as a path of least resistance to ice growth, potentially resulting in the observed morphology.

The observation of ice formation in CVS1 under isochoric conditions also indicates that the critical cooling rate of CVS1 may be slightly higher than suggested by the experiments of Powell-Palm et al. [15]. That study estimated the critical cooling rate to be approximately 100 °C/min, as that cooling rate resulted in no pressure increase while slightly slower cooling rates did. Our observations of ice formation in CVS1 indicate that pressure measurements may not be a sufficient indicator of full vitrification on its own. A rise in pressure rise indicates ice formation, but a lack of a pressure rise does not preclude ice formation. The vapor cavities in the 50 wt% DMSO solution suggest that ice could displace the vapor before generating a detectable pressure rise, as proposed by Solanki and Rabin [14]. Nevertheless, for volumes of ice large enough to generate detectable pressure, pressure measurements represent a simple and fast method for probing the formation and relative quantity of ice formed during cooling based on the magnitude of the pressure rise. The relationship between ice fraction and pressure in isochoric systems depends on multiple factors: the solution thermal contraction and compressibility; the specific volume of the system, which itself depends on conditions of the assembly; and lastly the

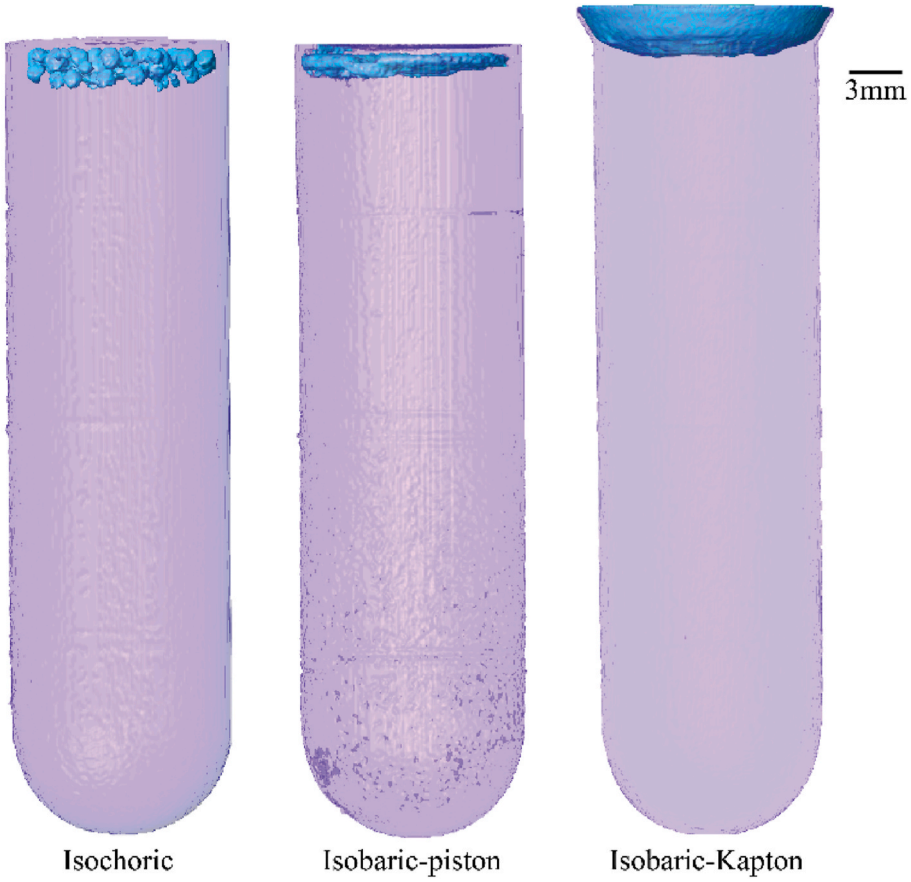

Fig. 6. Reconstructed CT scans of CVS1 in isochoric (left), isobaric-piston (center), and isobaric-Kapton (right) configurations. The vitrified solution and ice phases are segmented and shown in purple and blue, respectively. While a single mass of ice forms in the isobaric-piston system, many millimeter-scale ice globules form in the isochoric system. Slow cooling near the free interface in the isobaric-Kapton system results in significant ice formation that grows out of the measurement field of view. Ice volume fractions are reported in Table 2. (For interpretation of the references to colour in this figure legend, the reader is referred to the Web version of this article.)

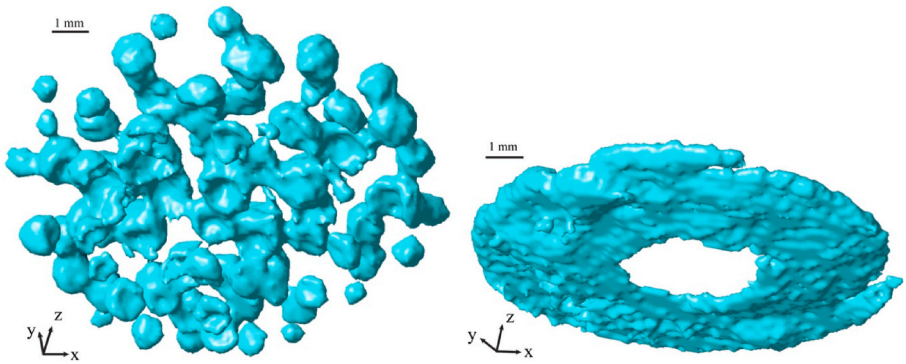

Fig. 7. Segmented ice phases from reconstructed CT scans of vitrified CVS1 in isochoric (left) and isobaric-piston (right) configurations. While a single solid mass of ice forms near the top of the chamber in the isobaric-piston system, millimeter-scale globular ice formations are observed in the isochoric system. This morphology is reminiscent of bubbles formed at randomly located nucleation sites during vapor cavitation or outgassing.

thermal contraction and compressibility of the chamber material. In the case of a highly contractile solution such as 50 wt% DMSO, up to approximately 6 % of the system may crystallize before an increase in pressure is detected based on the observed thermal contraction. In less contractile solutions such as CVS1, detection of much smaller volumes of ice may be possible. Future studies may seek to characterize the thermophysical properties of vitrification solutions in order to better understand volumetric and pressure responses during vitrification in isochoric systems.

3.3. *Cavity formation in isochorically confined aqueous solutions*

The observed ice morphology in the CVS1 solution suggests that fluid contraction during cooling may produce cavity formation. Equation (3) indicates that if the solution were to contract more than the chamber the pressure may drop rapidly. Should the pressure drop below a critical pressure, dissolved gases may come out of solution or the solution itself may cavitate. Studying the occurrence of cavitation would require up to O(1 MHz) frame rate measurements. Isochoric vitrification occurs in a thick-walled metal chamber, however, necessitating relatively long exposure periods with most in-lab X-ray sources. Cryogenic temperatures in a boiling nitrogen bath additionally hinder the use of acoustic inspection or accelerometers. High-speed synchrotron X-ray imaging could potentially be well suited for determining the presence of and studying cavitation during vitrification in isochorically confined systems.

If outgassing occurs, the morphology of rising bubbles in a fluid is a well understood function of the dimensionless Reynolds, Eotvos, and Morton numbers [29]. However, these parameters are difficult to estimate during vitrification as the kinematic viscosity of the fluid and the surface tension of the gas change rapidly with temperature and pressure. As a result, analytically or numerically confirming outgassing is challenging. Observing outgassing experimentally may be possible with slower frame rate in-lab imaging if the maximum outgassing rates are sufficiently slow. Should that be the case, it would be possible to rule out or confirm the presence of outgassing. We do not perform this step here as size constraints preclude us from placing the liquid nitrogen dewar in front of the X-ray source. As in the 50 wt% DMSO solution, the formation of vapor cavities would nullify the original isochoric confinement for the duration of their presence. Isochoric confinement could be restored should ice completely displace the vapor, for example. The presence of vapor does not imply that the system would necessarily be isobaric, however. During cavitation the pressure could change dramatically throughout the chamber, especially near the vapor cavity.

Pre-conditioning the solution would be one way to mitigate outgassing or cavitation. For example, one could apply freezing-rewarming cycles to the solution to degas the solution prior to cooling [30]. The isochoric system employed in this study closely emulates Berthelot tube systems used to study liquids at negative pressure [31–33]. In these studies, rigid containers are filled with a liquid and cooled, and in the absence of pre-existing bubbles or cavitation, the fluid can be metastably tensioned [34]. In order to generate these negative pressures, however, the system must be pre-conditioned by initially heating the sealed container in order to pressurize the liquid and force into solution any stubborn vapor trapped in crevices – which can act as a nucleation seed. Since this pre-conditioning would certainly injure any contained biological material, we do not perform this step in our experiments, nor was it part of the protocol employed in Ref. [15]. Alternatively, one could pre-compress the solution, choose a solution that contracts less than the chamber, or both.

4. Conclusions

Using a laboratory-scale photon counting X-ray CT system, we compare vitrification and ice formation processes in two aqueous solutions, CVS1 and 50 wt% DMSO, each under isochoric and isobaric conditions. We plunge cool these two solutions in liquid nitrogen (achieving cooling rates of roughly 110 °C/min) and evaluate the presence and volume fraction of glass, ice, and vapor phases after equilibration. A free air-liquid interface may result in local cooling rates dipping below the rate necessary for vitrification and cause significant ice formation, muddying the effects of confinement. After introducing a movable aluminum piston to match the thermal surface conditions of the isochoric confinement, we find that isochoric confinement yields similar volumes of ice (for CVS1) and vapor (for 50 wt% DMSO) compared to the isobaric configuration. Despite the similar ice volume fractions of the two configurations, we observe that isochoric vitrification of CVS1 produces a unique ice morphology that could be the result of outgassing or cavitation. Should that be the case, the solution would lose its initial isochoric confinement according to the definition in section 2.1. Pre-compressing the solution, adding an expanding material, choosing a solution whose thermal contraction is less than the chamber, or some combination thereof, is necessary to prevent outgassing or cavitation to maintain isochoric conditions during cooling.

Furthermore, our findings highlight the importance of aqueous solution and chamber thermo-mechanical properties for interpreting pressure measurements during vitrification in rigid isochoric systems. Without a better understanding of these properties, pressure measurements are best used as a quick tool for comparing formation of and relative volumes of ice formed so long as the ice volume is large enough to produce a pressure rise provided that the pressure sensor is not obstructed by a solid (amorphous or crystalline) and the entire stress tensor of the phase can be characterized by a pressure.

Additionally, the observation of unique ice morphologies motivates

future investigation of ice growth during vitrification in isochoric systems. The presence of ice acts to self-pressurize the system and the rejection of solutes from the growing ice phase would increase the concentration of the unfrozen solution, further modulating its melting point and passively diffusing additional solutes into the biomaterial [16, 35]. If the biospecimen is protected from an advancing ice front, the combined effects of higher pressure and increased solute concentration would increase the likelihood of successful vitrification in these portions of the systems.

Regarding the measurement system developed for this study, photon counting X-ray CT has proven to be a promising approach for the investigation of vitrification in aqueous systems. PCDs can produce a higher signal-to-noise ratio than traditional X-ray detectors, making them well suited for low contrast, high scatter systems such as isochoric thermodynamics. Moreover, traditional X-ray CT scans such as those done in Ref. [35]-[38] are not photon energy resolving, but photon counting X-ray CT can be. Due to this unique feature, photon counting X-ray CT could potentially identify different materials in a single CT scan by reconstructing each voxel's mass attenuation coefficient curves, identifying K-edges, or both. This capability could be used to quantitatively study processes such as the diffusion of CPAs into tissue and the formation of multiple thermodynamic phases simultaneously.

Lastly, the laboratory-scale system employed in this study images the chamber at a projection resolution of 98 μm in order to capture the full isochoric system in a single scan. More projections per rotation can improve the CT scan quality, although that was not necessary for this study. Opting for a smaller field of view would enable higher resolutions as the projection resolution scales linearly with magnification factor, M, and detector resolution. As an example, the current setup at $M = 10$ would yield a projected resolution of 17.2 μm. Volumes of ice at this scale are below the detectable limits possible with differential scanning calorimetry [36], as well as most visual [37] and X-ray diffraction [17] methods. Furthermore, assuming ideal conditions where phase segmentation is possible from single voxels, we can place a theoretical lower detection limit to volume fraction detection of $O(10^{-8})$ for this detector. Of course, realistically this number will be higher since more than one voxel is needed to confidently identify a phase distinction. Detectors with more pixels (and therefore more reconstructed voxels) would have lower limits. Photon counting X-ray CT can thus prove valuable for investigating further fundamental aspects of ice nucleation, growth, and vitrification.

Acknowledgements

This work received financial support from the National Science Foundation (NSF) Engineering Research Center for Advanced Technologies for Preservation of Biological Systems (ATP-Bio) under NSF EEC Grant No. 194154. Anthony Consiglio received additional support from the NSF Graduate Research Fellowship under Grant No. DGE 1752814. Simo Mäkiharju and Jason Parker also gratefully acknowledge the support of NSF EAGER award #1922877 program managers Ron Joslin and Shahab Shojaei-Zadeh, which enabled the development of the photon counting CT system. We would also like to thank Dr. Angel Rodriguez for his instrumental contributions to building the X-ray imaging system.

Appendix A. Supplementary data

Supplementary data to this article can be found online at https://doi.org/10.1016/j.cryobiol.2023.104839.

References

[1] S. Giwa, et al., The promise of organ and tissue preservation to transform medicine, Nat. Biotechnol. 35 (6) (2017) 530–542, https://doi.org/10.1038/nbt.3889.
[2] A.J. Hessheimer, F. Riquelme, Y. Fundora-Suárez, R. García Pérez, C. Fondevila, Normothermic perfusion and outcomes after liver transplantation, Transplant. Rev. 33 (4) (2019) 200–208, https://doi.org/10.1016/j.trre.2019.06.001.
[3] J. Brockmann, et al., Normothermic perfusion: a new paradigm for organ preservation, Ann. Surg. 250 (1) (2009) [Online]. Available: https://journals.lww.com/annalsofsurgery/fulltext/2009/07000/normothermic_perfusion__a_new_paradigm_for_organ.1.aspx.
[4] D.E. Pegg, Principles of cryopreservation, Cryopreserv. Free. Protoc. 368 (2007) 39–57, https://doi.org/10.1007/978-1-59745-362-2_3.
[5] C.A. Angell, Y. Choi, Crystallization and vitrification in aqueous systems, J. Microsc. 141 (3) (Mar. 1986) 251–261, https://doi.org/10.1111/j.1365-2818.1986.tb02720.x.
[6] P. Brüggeller, E. Mayer, Complete vitrification in pure liquid water and dilute aqueous solutions, Nature 288 (5791) (1980) 569–571, https://doi.org/10.1038/288569a0.
[7] G.M. Fahy, B. Wowk, in: W.F. Wolkers, H. Oldenhof (Eds.), Principles of Cryopreservation by Vitrification BT - Cryopreservation and Freeze-Drying Protocols, Springer New York, New York, NY, 2015, pp. 21–82, https://doi.org/10.1007/978-1-4939-2193-5_2.
[8] A. Consiglio, G. Ukpai, B. Rubinsky, M.J. Powell-Palm, Suppression of cavitation-induced nucleation in systems under isochoric confinement, Phys. Rev. Res. 2 (2) (2020), https://doi.org/10.1103/physrevresearch.2.023350.
[9] A.N. Consiglio, Y. Ouyang, M.J. Powell-Palm, B. Rubinsky, An extreme value statistics model of heterogeneous ice nucleation for quantifying the stability of supercooled aqueous systems, J. Chem. Phys. 159 (5) (2023).
[10] A.N. Consiglio, D. Lilley, R. Prasher, B. Rubinsky, M.J. Powell-Palm, Methods to stabilize aqueous supercooling identified by use of an isochoric nucleation detection (INDe) device, Cryobiology (2022), https://doi.org/10.1016/j.cryobiol.2022.03.003.
[11] M.J. Powell-Palm, B. Rubinsky, W. Sun, Freezing water at constant volume and under confinement, Commun. Phys. 3 (39) (2020), https://doi.org/10.1038/s42005-020-0303-9.
[12] B. Rubinsky, P.A. Perez, M.E. Carlson, The thermodynamic principles of isochoric cryopreservation, Cryobiology (2005), https://doi.org/10.1016/j.cryobiol.2004.12.002.
[13] Y. Zhang, et al., Isochoric vitrification: an experimental study to establish proof of concept, Cryobiology (2018), https://doi.org/10.1016/j.cryobiol.2018.06.005.
[14] P.K. Solanki, Y. Rabin, Is isochoric vitrification feasible? Cryobiology 111 (2023) 9–15, https://doi.org/10.1016/j.cryobiol.2023.03.007.
[15] M.J. Powell-Palm, et al., Cryopreservation and revival of Hawaiian stony corals using isochoric vitrification, Nat. Commun. 14 (1) (2023) 4859, https://doi.org/10.1038/s41467-023-40500-w.
[16] H.-M. Han, J. Huebinger, M. Grabenbauer, Self-pressurized rapid freezing (SPRF) as a simple fixation method for cryo-electron microscopy of vitreous sections, J. Struct. Biol. 178 (2) (2012) 84–87, https://doi.org/10.1016/j.jsb.2012.04.001.
[17] J.B. Hopkins, R. Badeau, M. Warkentin, R.E. Thorne, Effect of common cryoprotectants on critical warming rates and ice formation in aqueous solutions, Cryobiology 65 (3) (2012) 169–178, https://doi.org/10.1016/j.cryobiol.2012.05.010.
[18] Y. Rabin, Mathematical modeling of surface deformation during vitrification, Cryobiology 102 (Oct. 2021) 34–41, https://doi.org/10.1016/j.cryobiol.2021.07.014.
[19] D.M. Vispute, P.K. Solanki, Y. Rabin, Large surface deformation due to thermo-mechanical effects during cryopreservation by vitrification – mathematical model and experimental validation, PLoS One 18 (3) (Mar. 2023), e0282613, https://doi.org/10.1371/journal.pone.0282613 [Online]. Available:.
[20] P. Russo, Handbook of X-ray imaging: physics and technology, in: Series in Medical Physics and Biomedical Engineering, first ed., CRC Press, United States, 2018 https://doi.org/10.1201/9781351228251.
[21] J.T. Parker, S.A. Mäkiharju, Experimentally validated x-ray image simulations of 50 μm x-ray PIV tracer particles, Meas. Sci. Technol. 33 (5) (2022), 55301, https://doi.org/10.1088/1361-6501/ac4c0d.
[22] J.T. Parker, J. DeBerardinis, S.A. Mäkiharju, Enhanced laboratory x-ray particle tracking velocimetry with newly developed tungsten-coated O(50 μm) tracers, Exp. Fluid 63 (12) (2022) 184, https://doi.org/10.1007/s00348-022-03530-6.
[23] W. van Aarle, et al., The ASTRA Toolbox: a platform for advanced algorithm development in electron tomography, Ultramicroscopy 157 (2015) 35–47, https://doi.org/10.1016/j.ultramic.2015.05.002.
[24] W. van Aarle, et al., Fast and flexible X-ray tomography using the ASTRA toolbox, Opt Express 24 (22) (2016) 25129–25147, https://doi.org/10.1364/OE.24.025129.
[25] O. R. S. Inc., ORS Dragonfly, Canada, Montreal, 2020.
[26] B. Wowk, Thermodynamic aspects of vitrification, Cryobiology 60 (1) (2010) 11–22, https://doi.org/10.1016/j.cryobiol.2009.05.007.
[27] S. Gai, Z. Peng, B. Moghtaderi, J. Yu, E. Doroodchi, LBM study of ice nucleation induced by the collapse of cavitation bubbles, Comput. Fluids 246 (2022), 105616, https://doi.org/10.1016/j.compfluid.2022.105616.
[28] M.S. Barrow, P.R. Williams, H.-H. Chan, J.C. Dore, M.-C. Bellissent-Funel, Studies of cavitation and ice nucleation in 'doubly-metastable' water: time-lapse photography and neutron diffraction, Phys. Chem. Chem. Phys. 14 (38) (2012) 13255–13261, https://doi.org/10.1039/C2CP41925D.
[29] R. Clift, J.R. Grace, M.E. Weber, Bubbles, Drops, and Particles, 2005.
[30] Y. Rabin, J. Plitz, Thermal expansion of blood vessels and muscle specimens permeated with DMSO, DP6, and VS55 at cryogenic temperatures, Ann. Biomed. Eng. 33 (9) (2005) 1213–1228, https://doi.org/10.1007/s10439-005-5364-0.

[31] S.J. Henderson, R.J. Speedy, A Berthelot-Bourdon tube method for studying water under tension, J. Phys. Educ. 13 (7) (1980) 778, https://doi.org/10.1088/0022-3735/13/7/019.
[32] Y. Ohde, K. Hiro, M. Ono, H. Isono, H. Watanabe, Effects on trends in negative pressure of surface pre-treatments for the sealing plugs of a water-metal Berthelot tube system, J. Phys. D Appl. Phys. 25 (7) (1992) 1096, https://doi.org/10.1088/0022-3727/25/7/010.
[33] Y. Ohde, M. Ikemizu, H. Okamoto, W. Hosokawa, T. Ando, The two-stage increase in negative pressure with repeated cavitation for water in a metal Berthelot tube, J. Phys. D Appl. Phys. 21 (10) (1988) 1540, https://doi.org/10.1088/0022-3727/21/10/015.
[34] F. Caupin, Escaping the no man's land: recent experiments on metastable liquid water, J. Non-Cryst. Solids 407 (2015) 441–448, https://doi.org/10.1016/j.jnoncrysol.2014.09.037.
[35] B. Rubinsky, Mass transfer into biological matter using isochoric freezing, Cryobiology 100 (Jun. 2021) 212–215, https://doi.org/10.1016/j.cryobiol.2021.03.004.
[36] Z. Han, J.C. Bischof, CRITICAL COOLING AND WARMING RATES AS A FUNCTION OF CPA CONCENTRATION, 2020.
[37] J. Kangas, L. Zhan, Y. Liu, H. Natesan, K. Khosla, J. Bischof, Ultra-rapid laser calorimetry for the assessment of crystallization in low-concentration cryoprotectants, J. Heat Tran. 144 (3) (Feb. 2022), https://doi.org/10.1115/1.4052568.